Cerebral Cortex, April 2018;28: 1458–1471

doi: 10.1093/cercor/bhx357
Advance Access Publication Date: 17 January 2018
Original Article

ORIGINAL ARTICLE

Core Differences in Synaptic Signaling Between Primary Visual and Dorsolateral Prefrontal Cortex

Sheng-Tao Yang[1], Min Wang[1], Constantinos D. Paspalas[1], Johanna L. Crimins[1], Marcus T. Altman[1], James A. Mazer[1,2] and Amy F. T. Arnsten[1]

[1]Department of Neuroscience, Yale University School of Medicine, New Haven, CT 06510, USA and [2]Current address: Department of Cell Biology & Neuroscience, Montana State University, Bozeman, MT 59717, USA

Address correspondence to James A. Mazer, Department of Cell Biology and Neuroscience, Montana State University, Bozeman, MT 59717, USA. Email: james.mazer@montana.edu; Amy F. T. Arnsten, Department of Neuroscience, Yale Medical School, 333 Cedar St., New Haven, CT 06510, USA. Email: amy.arnsten@yale.edu

Abstract

Neurons in primary visual cortex (V1) are more resilient than those in dorsolateral prefrontal cortex (dlPFC) in aging, schizophrenia and Alzheimer's disease. The current study compared glutamate and neuromodulatory actions in macaque V1 to those in dlPFC, and found striking regional differences. V1 neuronal firing to visual stimuli depended on AMPA receptors, with subtle NMDA receptor contributions, while dlPFC depends primarily on NMDA receptors. Neuromodulatory actions also differed between regions. In V1, cAMP signaling increased neuronal firing, and the phosphodiesterase PDE4A was positioned to regulate cAMP effects on glutamate release from axons. HCN channels in V1 were classically located on distal dendrites, and enhanced cell firing. These data contrast with dlPFC, where PDE4A and HCN channels are concentrated in thin spines, and cAMP-HCN signaling gates inputs and weakens firing. These regional differences may explain why V1 neurons are more resilient than dlPFC neurons to the challenges of age and disease.

Key words: Alzheimer's disease, AMPA receptor, cAMP, NMDA receptor, V1

Introduction

The primary visual cortex (V1) and the dorsolateral prefrontal association cortex (dlPFC) have opposing functions: V1 neurons accurately signal the appearance of a visual stimulus, while dlPFC neurons encode visual information in the absence of sensory stimulation, that is, over the delay period in working memory tasks. Although higher cortical areas such as dlPFC likely contribute indirectly to "top-down" influences on V1 neurons (van Kerkoerle et al. 2017), for example, the differences between these neurons are still striking: V1 neurons start/stop firing within milliseconds (ms) of stimulus onset/offset (Bair et al. 2002), while dlPFC Delay cells are able to maintain firing across delay periods of 10–20 s in the absence of sensory stimulation (Wang et al. 2015), likely reflecting the more extensive recurrent excitatory networks in dlPFC. The fundamental differences in the response properties of V1 versus dlPFC neurons likely involve distinctly different molecular mechanisms for neurotransmission and neuromodulation, factors that may explain their disparate vulnerability to degeneration. For example, cognitive disorders such as schizophrenia and Alzheimer's disease are characterized by extensive atrophy of the layer III pyramidal cell circuits in dlPFC, while neurons in V1 are relatively spared (Lewis et al.

1987; Glantz and Lewis 2000). Similarly in aged monkeys there is extensive loss of dendritic spines in dlPFC, while spine density in V1 shows little decline with advancing age (Young et al. 2014). Are there molecular mechanisms that may help to explain the differential susceptibility of these cortical regions? Physiological characterizations of the macaque V1 or dlPFC, to date explored by separate fields, have provided suggestive data that neurotransmission differs between primary sensory cortex and high order association cortical circuits. The current study directly compared the molecular bases of synaptic transmission and neuromodulation in these cortical regions by applying experimental protocols previously used to characterize Delay cells in dlPFC, to neurons in primate V1.

Studies of primary visual cortex in rodents have revealed classical glutamate neurotransmission in V1. AMPA receptors (AMPAR) play a large role and provide rapid synaptic transmission, while the role of NMDA receptors (NMDAR) is subtler and comes into play when AMPAR depolarization relieves the magnesium block of NMDAR (Langdon and Sur 1992). The NMDAR subtypes mediating neurotransmission in V1 change over the developmental period, similar to those seen in hippocampus or somatosensory cortex (Liu et al. 2004), where the slower, NR2B subunits are less evident in the adult and are replaced by NMDAR with faster, NR2A subunits (Nase et al. 1999). NMDAR with NR2B have been shown to play an important role in plastic changes in rodent V1 circuits during development (Berardi et al. 2003; Li and Wang 2013), in addition to classic cAMP-PKA signaling events that can strengthen connections (Berardi et al. 2003). Although the ratio of NMDAR/AMPAR ratio appears similar between V1 and medial PFC in the rodent (Myme et al. 2003), there is less NR2B expression in V1 compared with the medial PFC (Wang et al. 2008), where NMDAR currents have been related to the recurrent firing needed for working memory (Wang et al. 2008).

Although there are only a few studies of neurotransmission in V1 of rhesus macaques, this research has provided a detailed picture of how the mechanics of neurotransmission relate to the processing of visual stimuli, including differences between "bottom-up" sensory signaling and "top-down" attention. Studies of glutamate receptor mechanisms in primates are generally consistent with those in rodents (Self et al. 2012). This seminal work found that AMPARs play a large role in rapid, feedforward "bottom-up" processing, while NMDARs are more important for recurrent "top-down" influences, for example, as tested by figure-ground modulation (Self et al. 2012). Attentional modulation in visual cortex depends on both glutamate and cholinergic actions: NMDAR are especially important for mediating firing rate variance, noise correlation, and LFP gamma power (Herrero et al. 2013), while acetylcholine has been shown to induce multiplicative gain changes through the action of muscarinic receptors (Herrero et al. 2008). In primate V1, selective blockade of NMDAR with NR2B subunits may even increase feedforward, "bottom-up" sensory processing (Self et al. 2012); but in rat V1, blockade of presynaptic NR2B may inhibit glutamate release (Li et al. 2009).

In contrast, a very different picture of synaptic transmission and modulation has emerged in the primate dlPFC, where extensive recurrent connections underlie the persistent firing of Delay cells in monkeys performing visuospatial working memory tasks (Goldman-Rakic 1995). The task-related firing of Delay cells is only subtly reduced by AMPAR blockade, but instead depends on NMDAR-NR2B, which are found exclusively in the postsynaptic density (PSD) (Wang et al. 2013). The permissive depolarization required for NMDA action is mediated by cholinergic stimulation of nicotinic α7 receptors, which are localized in the glutamatergic PSD (Yang et al. 2013). Importantly, there is extensive evidence that feedforward calcium-cAMP-PKA activity in dendritic spines weakens synaptic connectivity and results in reduced dlPFC Delay cell firing via cAMP-PKA mediated opening of nearby HCN and KCNQ channels (Vijayraghavan et al. 2007; Wang et al. 2007, 2011; Arnsten et al. 2012; Gamo et al. 2015). Thus, while HCN channels are classically localized on the distal dendrites of pyramidal cells (Lörincz et al. 2002), where they open under conditions of hyperpolarization (He et al. 2014), in layer III of dlPFC immunoelectron microscopy (immunoEM) shows these channels are preferentially found on long, thin spines, where they can interact with a constellation of cAMP-signaling proteins including the phosphodiesterase PDE4A (Paspalas et al. 2013). cAMP signaling increases the fraction of open state HCN channels, rapidly gating out network inputs and providing a "signature of flexibility" (Wang et al. 2007). High levels of cAMP-HCN signaling during acute stress exposure (Arnsten 2015) or with advancing age (Wang et al. 2011) in part leads to a reduction in dlPFC Delay cell firing. In rats, chronic stress increases cAMP-calcium signaling in PFC resulting in a loss of spines (Hains et al. 2009, 2015). Dysregulation of cAMP-calcium signaling in the aged dlPFC contributes to phosphorylation of tau (Carlyle et al. 2014). Thus, these powerful actions appear to contribute to the vulnerability of PFC circuits, and may differentiate them from the relative resilience of primate V1. However, it is not known how cAMP or HCN channel signaling affects neuronal firing in primate V1, nor the precise cellular localization of cAMP signaling proteins and HCN channels in primate V1 neurons.

In this study we examined NMDAR (including NMDAR-NR2B), AMPAR/kainate receptor (KR), cAMP-PKA and HCN channel mechanisms in primate V1, using the same pharmacological agents and immunoEM approaches used previously in dlPFC to facilitate direct comparisons between the 2 cortical regions. We also compared V1 neurons to both dlPFC Delay cells, which exhibit sustained activity in the absence of sensory stimulation, and the rarer dlPFC Cue cells, that fire only when a visual cue is present (Funahashi et al. 1989), that is, more like V1 neurons, to determine whether differences in drug response were due to cortical region or to neuronal function. We found that sensory signals in V1 are modulated in a classic manner, opposite to dlPFC Delay cells, while modulation of dlPFC Cue cell activity shows similarities to both V1 and dlPFC Delay cells. In particular, V1 neuronal firing was enhanced by cAMP and HCN channel signaling, which may help to explain why V1 circuits are more resilient than dlPFC Delay cells to the deleterious effects of stress and age.

Materials and Methods

All procedures were in accordance with the NIH Guide for the Care and Use of Laboratory Animals and approved by the Yale University Institutional Animal Care and Use Committee.

Electrophysiology

Fixation Task

Monkeys performed a visual fixation task (Fig. 1) while we recorded from single neuron in V1 and performed iontophoresis experiments. Prior to the start of these experiments, animals were implanted with a head fixation device and a recording chamber (see below). Animals were trained to grasp and hold a touch bar and maintain fixation on a 2–3 arcmin 100% contrast square fixation target for up to 7 s. Eye movements >1° from the fixation target aborted the trial. After a random time interval (truncated exponential distribution, mean = 6.5 s), the fixation

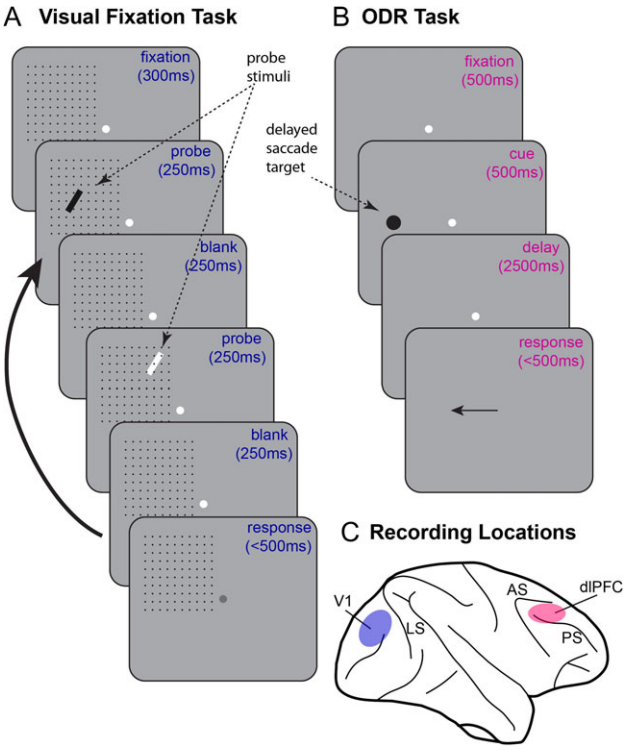

Figure 1. Recording paradigm. (A) The behavioral task used to map receptive fields (RFs) in primary visual cortex (V1). Monkeys passively viewed probe stimuli (10–20 Hz) flashed in and around the RF while detecting a small change in the luminance of the fixation spot. Responses to probe stimuli (white or black, indicated by black arrows) were used to assess neuronal responsivity during drug application. The grid was invisible to monkeys. (B) The oculomotor delayed response (ODR) task used to assess visual spatial working memory during recordings from the dorsolateral prefrontal cortex (dlPFC). The location of a brief, spatial cue had to be remembered over a delay period to guide a saccadic response to the remembered location. The position of the cue randomly varied over 8 spatial locations. (C) The recording locations in V1 (blue) and in dlPFC (pink). LS, lunate sulcus; AS, arcuate sulcus; PS, principal sulcus.

target dimmed slightly (10% or less) and animals had to release the touch bar within 500 ms to obtain a liquid reward. Following fixation breaks, premature (<70 ms) and late (>500 ms) touch bar responses, the display was briefly flashed red to indicate an error, followed by a 1–2 s timeout period. During the fixation period, before dimming of the fixation spot, 100% contrast black and white probe stimuli (Fig. 1A) were flashed in randomized order on an invisible 10 × 10 grid at 5–10 Hz to map the spatial RF of each neuron studied. The black probe stimuli were filled with 100% contrast black color, while white probe stimuli filled with 100% contrast white color, as illustrated in Figure 1A. Preliminary hand mapping was used to select the orientation, length and width of the probe to optimize parameters for each cell. The probe sequence had a 50% duty cycle, with a blank period between each probe presentation. Probes were presented on a uniform gray background (26.3 cd/m^2) and black and white probes were 0.02 and 51.5 cd/m^2, respectively, on a linearized display with a 60 or 70 Hz refresh rate. The approximate receptive field (RF) boundaries were mapped by hand and used to position the 10 × 10 grid. Mean response to probes at each grid position were calculated used to find the half-maximal iso-response contour, which was then fit with a circle (Mazer et al. 2002; Touryan and Mazer 2015) to quantify the location and size of the RF. Black and white probes were presented at least once at each grid point in a block of trials and each experimental condition (control or drugs) contained at least 4 blocks. Poststimulus time histograms (PSTH) were constructed by averaging cell responses across all probe positions and all blocks for a given experimental condition.

Data Collection

Data were collected from 2 adult (ages 14 and 9) male rhesus monkeys (*Macaca mulatta*), 13–15 kg. Animals were prepared for experiments by implanting a head fixation device and a recording chamber in 2 separate sterile surgeries. First we attached a custom made Titanium headpost (AZ Machining, Boston, MA) to the skull using cortical bone screws (Synthes, West Chester, PA) under isoflurane anesthesia. Following osseointegration, acclimation to head restraint and subsequent behavioral training on the visual fixation task described above, a 12-mm diameter craniotomy was performed over area V1 and a stainless steel 14 mm diameter recording chamber was attached directly to the bone surrounding the craniotomy to provide electrode access. The chamber was secured to the skull using additional bone screws and acrylic cement (Densply-Caulk, Milford, DE). V1 was targeted using stereotaxic coordinates and skull morphology and subsequently confirmed based on physiological properties of recorded cells (i.e., neuronal response latency, RF size, and visual field eccentricity) (Mazer et al. 2002).

Task timing, stimulus presentation and data collection were controlled by a Linux PC running pype (https://github.com/mazerj/pype3). Stimuli were presented on a gamma corrected (linearized) display (Viewsonic G810 CRT display, 85 Hz or BenQ XL2720Z, 60 Hz) at a effective resolution of 1025 × 768 pixels viewed at a distance of 66 cm (20 pixels/deg). Eye movements were recorded digitally at a minimum of 500 or 1000 Hz using an infrared eye tracker (EyeLink 1000, SR Research, Toronto, Canada), and single neuron activity was recorded with iontophoretic electrodes. Iontophoretic electrodes were constructed by inserting a 20-μm-pitch carbon fiber (ELSI, San Diego, CA) into the central barrel of a 7-barrel nonfilamented capillary glass (Friedrich and Dimmock, Millville, NJ). The assembly was then pulled using a custom electrode puller (PMP-107, Microdata Instrument Inc., South Plainfield, NJ) and the tip was beveled to obtain the finished electrode. Finished electrodes had impedances of 0.3–1.0 MΩ (at 1 kHz) and tip sizes of 30–40 μm. The outer barrels of the electrode were then filled with drug solutions and the solutions were pushed into the tip of the electrode using compressed air. The electrode was inserted into a sharpened hypodermic guide tube that was used to penetrate the dura mater. Electrodes were then advanced into the brain with a custom made motorized microdrive (MM-3M-F, National Aperture, Nashua, NH). Neural signals were amplified, filtered and discriminated (RZ5, Tucker-Davis Technologies, Alachua, FL) and spike times were recorded with 1 ms precision.

This study used iontophoresis to apply charged pharmacological agents directly onto the recorded V1 neurons. Since this method does not require volume fluid injection, it is possible to maintain stable neuronal recordings for long periods of time while simultaneously applying various drugs. The minute amount of drugs applied here as sufficiently small as to have no effect on behavior. The following pharmacological agents were used: AMPA/kainate receptor antagonist CNQX disodium salt (CNQX), NMDA receptor antagonist MK801 maleate (MK), NMDA NR2B receptor antagonist Ro25-6981 maleate (Ro), cAMP analog 8-Br-cAMP sodium salt (8-Br), hyperpolarization-activated cyclic nucleotide-gated (HCN) cation channels blocker ZD7288 (ZD). All agents were purchased from Tocris Bioscience and dissolved at

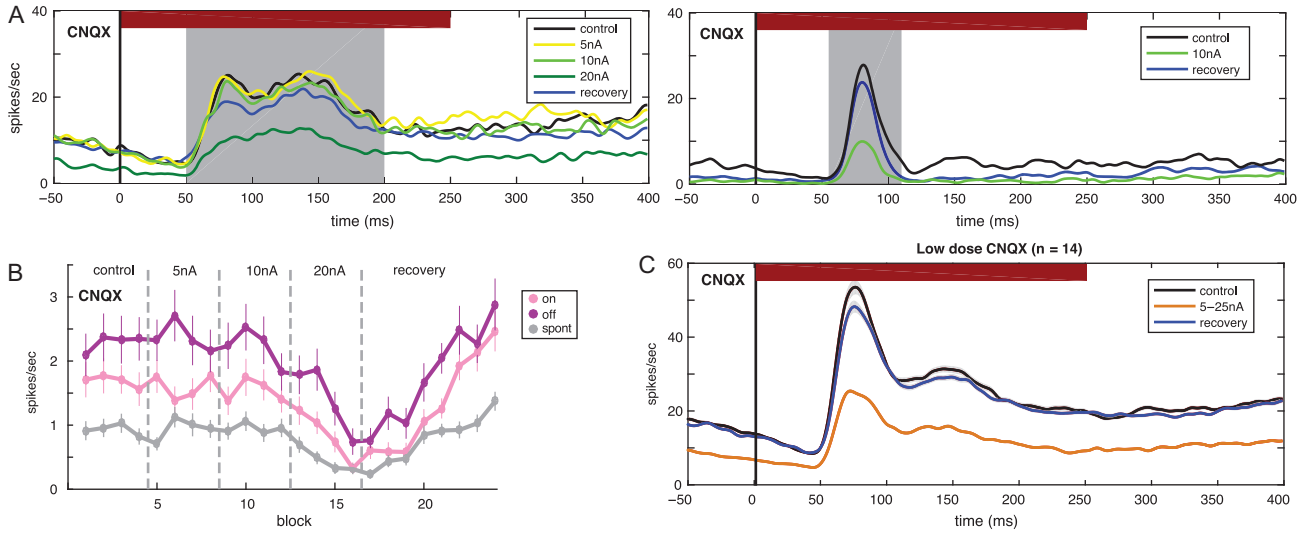

Figure 2. Iontophoresis of the AMPA receptor antagonist, CNQX in V1. (*A*) *Left*: an example neuron showing the effects of increasing doses of CNQX (5–20 nA) on neuronal firing. The highest dose of CNQX (20 nA, dark green) significantly decreased the visual response (control vs. 20 nA, one-way ANOVA, $F_{1,1888} = 76.2378$, $P < 0.001$); this decrease was recovered when drug was removed (recovery vs. 20 nA, one-way ANOVA, $F_{1,1930} = 132.8902$, $P < 0.001$). *Right*: another example neuron showing that lower dose of CNQX (10 nA, light green) significantly decreased the visual response (control vs. 10 nA, one-way ANOVA, $F_{1,2164} = 45.852$, $P < 0.001$); this decrease was recovered when drug was removed (recovery vs. 10 nA, one-way ANOVA, $F_{1,1764} = 75.4852$, $P < 0.001$). The visual probe was presented from time 0 to 250 ms, indicated by the red bar. The area indicated by the gray bar was defined as the visual response and was used for statistical analysis. (*B*) The same cell as in (*A*) left, showing firing dynamics during application of increasing doses of CNQX. Visual responses are classified as "On responses" to a luminance increment (pink line), "Off responses" to a luminance decrement (purple line), and spontaneous firing (spont, gray line). Each dot shows the neuron's response averaged across one block. Error bars indicate standard error of the mean (SEM). Vertical dashed lines separate differing drug conditions. (*C*) Population analysis (average of 14 neurons) of low doses of CNQX. Low doses of CNQX (5–25 nA) significantly decreased neuronal firing (control vs. CNQX, two-tailed paired *t*-test, tdep(13) = 5.114, $P < 0.001$, $n = 14$); firing significantly increased following removal of drug (recovery vs. CNQX, two-tailed paired *t*-test, tdep(13) = 2.652, $P < 0.05$, $n = 14$). Visual response from time 50 to 200 ms are selected for significance test (two-tailed paired *t*-test) in population analysis. Black, control; gold, low dose of CNQX; blue, recovery. Gray shading, SEM.

10 mM (in saline for ZD, in water for all others). A NeuroPhore BH-2 iontophoretic system (Harvard Apparatus, Holliston, MA) was used to control drug delivery. The drugs CNQX and 8-Br were ejected at negative currents that ranged from −5 to −50 nA, and positive retaining currents of 5 nA were used in a cycled manner (1 s on, 1 s off) when not applying drugs. The drugs Ro, MK and ZD were ejected at positive currents and retained at negative currents. Please note that iontophoresis of saline had no effect on neuronal firing (Wang et al. 2013), indicating that the electrical current alone does not alter neuronal firing. Consistent with these previous studies, currents used for drug ejection did not affect neuronal recordings in the current study, and we observed no systematic changes in either spike amplitude or time course at any ejection current level.

Data Analysis

We used one-way ANOVA with repeated measures to assess the statistical significance of each drug's effect by comparing each neuron's visual response during control, drug application and recovery periods. For analyses of the entire population of neurons for each drug condition, we used a two-tailed paired *t*-test to test for significant differences between drug versus control or recovery. Visual responses were estimated by computing the firing rate in the period 50–200 ms after probe onset. Only neurons with visual driven responses (based on a two-tailed *t*-test comparing prestimulus and poststimulus average firing rate) were included in the population analysis.

Immunocytochemistry

Two female young-adult (ages 7 and 9) rhesus macaques were anesthetized with sodium pentobarbital (30 mg/kg, i.v.), and perfused transcardially with 4% paraformaldehyde/0.05% glutaraldehyde, plus 0.2% picric acid in 0.1 M phosphate buffer. The brains were blocked coronally, vibrosliced at 70 µm, cryoprotected in sucrose, and stored at −80 °C. Sections of V1 corresponding to the rostral half of the calcarine sulcus were thawed and processed for PDE4A or HCN1 channel immunocytochemistry. The histological and immunocytochemical procedures, and all specificity tests, have been described in detail in Paspalas et al. (2013).

HCN1 channel immunolabeling used rabbit antibodies against the human HCN1 channel subunit (HPA019195, Atlas, Bromma, Sweden). Liquid-phase adsorption of the anti-HCN1 with the immunizing peptide (5–15 µg/ml; APrEST72946; Atlas) eliminated all labeling. PDE4A in V1 was labeled and quantified as in dlPFC (Carlyle et al. 2014) to allow cortical area comparisons. For channel immunolabeling, we used rabbit antibodies against the human HCN1 channel subunit (HPA019195, Atlas, Bromma, Sweden). Briefly, sections were incubated for 48 h at 4 °C in anti-PDE4A (1:300; ab14607, Abcam, Cambridge, MA) or anti-HCN1 (1:1000) in tris-buffered saline (TBS), and transferred for 2 h into species-specific biotinylated F(ab′)$_2$ fragments (1:500 in TBS; Jackson Immunoresearch, West Grove, PA), and finally into avidin–biotinylated peroxidase (1:200 in TBS; Vector Laboratories, Burlingame, CA). Peroxidase activity was visualized in 0.05% diaminobenzidine (DAB) in TB with the addition of 0.01% hydrogen peroxide.

Results

Physiology

Single neuron recordings combined with iontophoresis were used to examine the molecular regulation of V1 neurons during

visual processing. Monkeys performed a visual fixation task where probe stimuli (5–10 Hz) were flashed in and around the neuron's RF while the animals maintained gaze on a central fixation spot in order to detect and report the occurrence of a small luminance decrement (Fig. 1A). This contrasts with the visuospatial working memory task used to assess dlPFC neurons, where monkeys were required to remember the spatial position of a transient visual cue over a brief delay (Fig. 1B). Recordings were made from the primary visual cortex (V1), shown in blue (Fig. 1C), and compared with previous recordings from the dlPFC surrounding the principal sulcus (Fig. 1C, red).

We studied a total of 108 V1 neurons from 2 monkeys (76 neurons from Monkey R, 32 neurons from Monkey B; including 14 neurons for CNQX experiment, 16 neurons for MK experiment, 20 neurons for Ro experiment, 23 neurons for 8-Br experiment, 35 neurons for ZD experiment) performing the visual fixation task. Preliminary analysis revealed no significant differences between the 2 animals (response differences between drug effect and control of neurons in Monkey R vs. those differences in Monkey B, one-way ANOVA, $F_{1,106} = 0.3122$, $P = 0.5775$, $n = 108$), and thus the data were combined. We also recorded 8 dlPFC neurons from Monkey C (8 neurons for 8-Br experiment) performing the oculomotor delayed response (ODR) task used to assess visual spatial working memory (Fig. 1B) (Wang et al. 2013).

Role of AMPA Receptors

The contribution of AMPAR/KR stimulation was assessed by iontophoretic application of the AMPAR/KR antagonist CNQX disodium salt (CNQX). Iontophoresis of CNQX produced a potent, dose-related reduction in the evoked response to visual stimuli in V1 neurons (Fig. 2). As illustrated in 2 example neurons (Fig. 2A), even relatively low doses of CNQX (10–20 nA) markedly decreased neuronal firing (Fig. 2A; left panel: control vs. 20 nA, one-way ANOVA, $F_{1,1888} = 76.2378$, $P < 0.001$; right panel: control vs. 10 nA, one-way ANOVA, $F_{1,2164} = 45.852$, $P < 0.001$). After stopping application of CNQX, neuronal firing gradually recovered to baseline levels (Fig. 2A,B; left panel: recovery vs. 20 nA, one-way ANOVA, $F_{1,1930} = 132.8902$, $P < 0.001$; right panel: recovery vs. 10 nA, one-way ANOVA, $F_{1,1764} = 75.4852$, $P < 0.001$) confirming that changes in responsivity were due to the specific action of the drug and not changes in neuronal health or other nonspecific factors (Fig. 2B). We found similar effects of CNQX on responses to luminance increments (On response, 59.06 ± 5.96%) and decrements (Off response, 56.89 ± 6.39%) (drug effect on On response vs. Off response, two-tailed paired t-test, tdep(13) = 0.8206, $P = 0.4267$, $n = 14$).

A combination of all neurons at low doses CNQX data (5–25 nA) showed an overall significant reduction in firing (Fig. 2C; control vs. CNQX, two-tailed paired t-test, tdep(13) = 5.114, $P < 0.001$, $n = 14$), which normalized after removal of the drug (Fig. 2C; recovery vs. CNQX, two-tailed paired t-test, tdep(13) = 2.652, $P < 0.05$, $n = 14$). Thus, AMPAR/KR blockade resulted in a potent reduction in the responsivity of V1 neurons to visual stimuli.

The doses of CNQX that attenuated visual responses in V1 also reduced the level of spontaneous activity (defined as the period from 200 ms before stimulus onset to stimulus onset), although the observed change in spontaneous activity was less than the change in sensory-evoked firing (spontaneous, reduced to 65.36 ± 8.26% of control; visually evoked, reduced to 59.17 ± 5.27% of control; spontaneous vs. visually evoked, two-tailed paired t-test, tdep(13) = 2.3137, $P < 0.05$, $n = 14$), consistent with a change in neuronal gain. These data suggest that the basal firing of the canonical cortical circuit in V1 involves AMPAR/KR stimulation, which is amplified during periods of visual stimulation.

Role of NMDA Receptors

The contribution of NMDAR activity in general was tested with iontophoretic application of the noncompetitive NMDAR antagonist, (+)-MK801 maleate (MK; Fig. 3A–D). MK801 produced a dose-related reduction in firing, but higher dosages were required to cause rate reduction (≥25 nA), as illustrated by the example neurons shown in Figure 3A,B. For the neuron illustrated in the left panel of Figure 3A, 15 nA MK801 had no effect on visual responses, while at 25 nA visual responses were slightly attenuated and at 35 nA they were significantly decreased (control vs. 35 nA, one-way ANOVA, $F_{1,1614} = 63.413$, $P < 0.001$). Visual responses returned toward baseline levels when drug application was halted (Fig. 3A left panel; recovery vs. 35 nA, one-way ANOVA, $F_{1,1794} = 23.8717$, $P < 0.001$), consistent with drug-induced actions. The effects of MK were similar in the neuron depicted in the right panel of Figure 3A, although in this case a 50 nA dose was required to elicit a significant decrease in firing (Fig. 3A right panel; control vs. 50 nA, one-way ANOVA, $F_{1,988} = 112.4641$, $P < 0.001$). Again, responses returned toward normal once drug application was halted (Fig. 3A right panel; recovery vs. 50 nA, one-way ANOVA, $F_{1,1101} = 111.4134$, $P < 0.001$). Population analysis of all neurons tested with MK showed that low doses of MK (10–25 nA) did not significantly alter neuronal firing (Fig. 3C; control vs. low dose MK, two-tailed paired t-test, tdep(10) = 0.4223, $P = 0.6817$, $n = 11$), while higher doses (35–50 nA) significantly decreased neuronal firing (Fig. 3D; control vs. high dose MK, two-tailed paired t-test, tdep(15) = 4.246, $P < 0.001$, $n = 16$). As in the case of AMPAR/KR, application of MK at doses high enough to reduce visual responses also reduced spontaneous activity, and the effect of MK on spontaneous activity was weaker than its effect on visually evoked activity (spontaneous, reduced to 59.58 ± 6.04% of control; visually evoked, reduced to 53.79 ± 6.42% of control; spontaneous vs. visually evoked, two-tailed paired t-test, tdep(15) = 3.15, $P < 0.01$, $n = 16$). Across the population of neurons studied, the effects of MK washed out once drug application was stopped (Fig. 3D; recovery vs. high dose MK, two-tailed paired t-test, tdep(15) = 3.195, $P < 0.01$, $n = 16$). As shown in Figure 3B, MK attenuated responses to both luminance increments and decrements (On response, 52.05 ± 5.77%; Off response, 52.15 ± 5.62%; On response vs. Off response, two-tailed paired t-test, tdep(15) = –0.0999, $P = 0.9217$, $n = 16$).

The contribution of NMDAR with NR2B subunits was examined by applying an NMDAR-NR2B specific blocker, Ro25-6981 (Ro). Figure 3E,F demonstrates that low doses of Ro were ineffective, but at higher doses visual responses were reduced. For the example neuron shown in the left panel of Figure 3E, low doses of Ro25-6981 (10–20 nA) had no effect on neuronal firing, while a higher dose (30 nA) produced a small but significant decrease in the visual response (Fig. 3E, left panel; control vs. 30 nA, one-way ANOVA, $F_{1,2017} = 45.8612$, $P < 0.001$). As with CNQX and MK, neuronal firing rates were restored to baseline levels during the recovery period (recovery vs. 30 nA, one-way ANOVA, $F_{1,2041} = 16.0743$, $P < 0.001$). A second example neuron was even less sensitive to Ro25-6981, where 60 nA was needed to reduce firing (Fig. 3E, right panel; control vs. 60 nA, one-way ANOVA, $F_{1,1949} = 13.1351$, $P < 0.001$). Neuronal firing recovered when drug was no longer applied (recovery vs. 60 nA, one-way

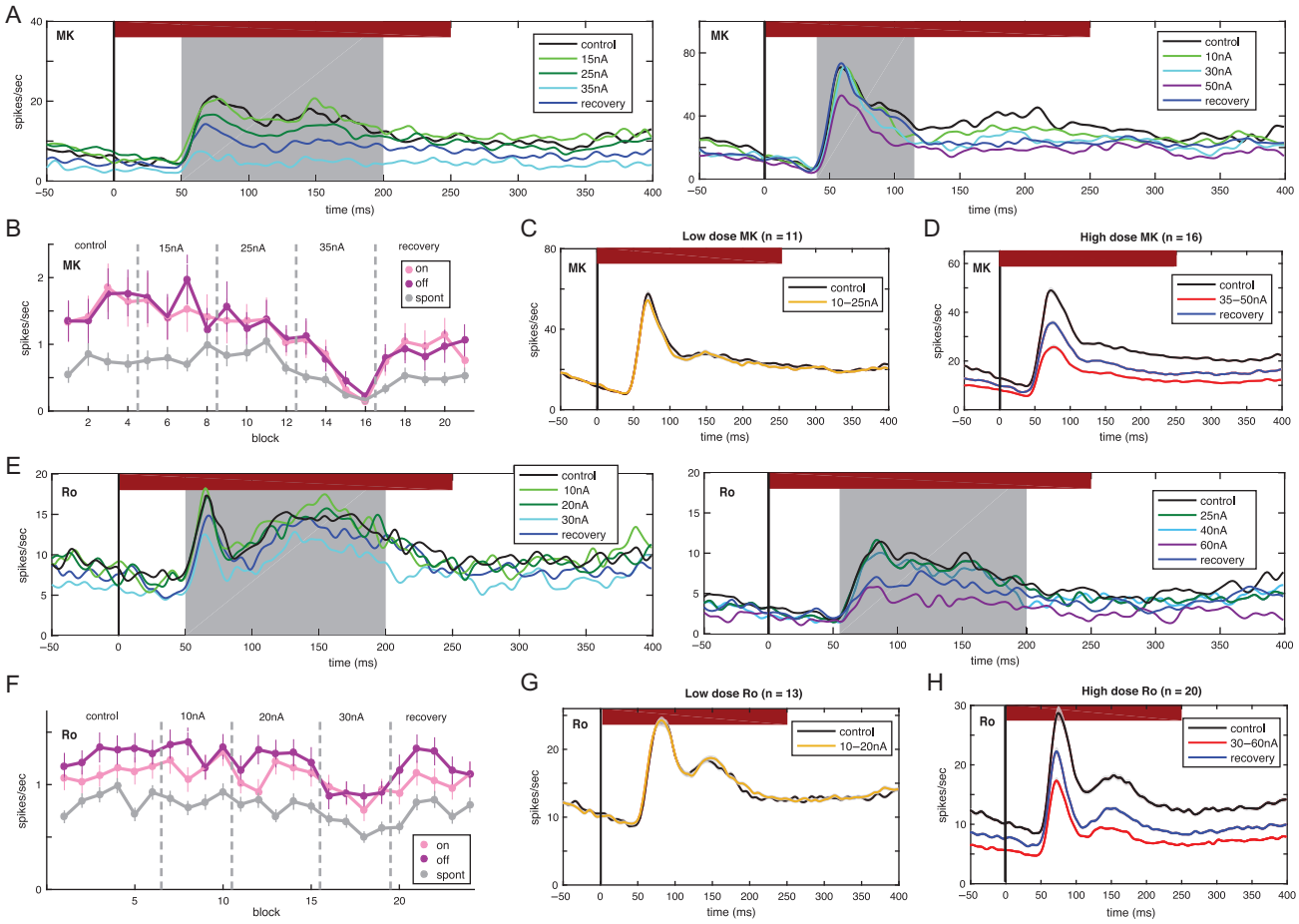

Figure 3. Iontophoresis of the general NMDA receptor antagonist, MK801 (MK), or the NMDA-NR2B selective antagonist, Ro25-6981 (Ro) in V1. (*A*) *Left*: an example neuron showing the effects of increasing doses of MK (15–35 nA) on neuronal firing. The highest dose of MK (35 nA, cyan) significantly decreased the visual response (control vs. 35 nA, one-way ANOVA, $F_{1,1614} = 63.413$, $P < 0.001$); this decrease was recovered when drug was removed (recovery vs. 35 nA, one-way ANOVA, $F_{1,1794} = 23.8717$, $P < 0.001$). *Right*: another example neuron showing that higher dose of MK (50 nA, purple) decreased firing (control vs. 50 nA, one-way ANOVA, $F_{1,988} = 112.4641$, $P < 0.001$); this decrease was recovered when drug was removed (recovery vs. 50 nA, one-way ANOVA, $F_{1,1101} = 111.4134$, $P < 0.001$). (*B*) The same cell as in (*A*) left, showing firing dynamics during application of increasing doses of MK. (*C*) Population analysis (average of 11 neurons) of low doses of MK. Low doses of MK (10–25 nA) did not change neuronal firing (control vs. low dose MK, two-tailed paired *t*-test, tdep(10) = 0.4223, $P = 0.6817$, $n = 11$). Black, control; gold, low dose of MK. (*D*) Population analysis (average of 16 neurons) to high doses of MK. Higher doses (35–50 nA) significantly decreased neuronal firing (control vs. high dose MK, two-tailed paired *t*-test, tdep(15) = 4.2606, $P < 0.001$, $n = 16$); firing significantly increased following removal of drug (recovery vs. high dose MK, two-tailed paired *t*-test, tdep(15) = 3.195, $P < 0.01$, $n = 16$). (*E*) *Left*: an example neuron showing the effects of increasing doses of ro (10–30 nA) on neuronal firing. The highest dose of Ro (30 nA, cyan) significantly decreased the visual response (control vs. 30 nA, one-way ANOVA, $F_{1,2017} = 45.8612$, $P < 0.001$); this decrease was recovered when drug was removed (recovery vs. 30 nA, one-way ANOVA, $F_{1,2041} = 16.0743$, $P < 0.001$). Right: another example neuron showing that higher dose of ro (60 nA, dark purple) significantly decreased the visual response (control vs. 60 nA, one-way ANOVA, $F_{1,1949} = 13.1351$, $P < 0.001$); this decrease was recovered when drug was removed (recovery vs. 60 nA, one-way ANOVA, $F_{12154} = 3.8558$, $P < 0.05$). (*F*) The same cell as in (*A*) left, showing firing dynamics during application of increasing doses of ro. (*G*) Population analysis (average of 13 neurons) of low doses of ro. Low doses of ro (10–20 nA) did not change neuronal firing (control vs. low dose Ro, two-tailed paired *t*-test, tdep(12) = –0.8109, $P = 0.4332$, $n = 13$). Black, control; gold, low dose of ro. (*H*) Population analysis (average of 20 neurons) to high doses of ro. Higher doses (30–60 nA) significantly decreased neuronal firing (control vs. high dose Ro, two-tailed paired *t*-test, tdep(19) = 8.632, $P < 0.001$, $n = 20$); firing significantly increased following removal of drug (recovery vs. high dose Ro, two-tailed paired *t*-test, tdep(19) = 2.1528, $P < 0.05$, $n = 20$).

ANOVA, $F_{1,2154} = 3.8558$, $P < 0.05$). Population analysis of all neurons tested showed that low doses of Ro (10–20 nA) did not alter neuronal firing (Fig. 3*G*; control vs. low dose Ro, two-tailed paired *t*-test, tdep(12) = 0.8109, $P = 0.4332$, $n = 13$), while higher doses (30–60 nA) significantly decreased neuronal firing (Fig. 3*H*; control vs. high dose Ro, two-tailed paired *t*-test, tdep(19) = 8.632, $P < 0.001$, $n = 20$). Ro doses that reduced sensory responses also reduced spontaneous activity, but again to a lesser extent (spontaneous, 67.68 ± 4.83% of control; visually evoked, 61.66 ± 3.11% of control; spontaneous vs. visually evoked, two-tailed paired *t*-test, tdep(19) = 2.9627, $P < 0.01$, $n = 20$). As with the example neuron, firing increased and returned to control levels once drug application was stopped (Fig. 3*H*; recovery vs. high dose Ro, two-tailed paired *t*-test, tdep(19) = 2.1528, $P < 0.05$, $n = 20$). Ro responses were similar for luminance increment and decrement stimuli (On response, 60.94 ± 3.2%; Off response, 62.49 ± 3.22%; On response vs. Off response, two-tailed paired *t*-test, tdep(19) = –0.9872, $P = 0.336$, $n = 20$), as shown in Figure 3*F*.

Direct comparisons of low doses (20–25 nA) of CNQX versus Ro25-6981 showed that V1 neuronal firing was more sensitive to AMPAR/KR than NMDA receptor blockade. Low doses of CNQX significantly reduced firing by a factor of two, relative to control levels (58.26 ± 5.97% of control, control vs. CNQX, two-tailed paired *t*-test, tdep(9) = –6.9847, $P < 0.001$, $n = 10$), while the same doses of Ro25-6981 had little effect on V1 neurons

(104.09 ± 4.09% of control, control vs. Ro, two-tailed paired *t*-test, tdep(10) = −0.9781, $P = 3511$, $n = 11$; Fig. 4A), indicating that visual responses in V1 are particularly dependent on AMPAR/KR stimulation. This is opposite to the pattern observed in Delay cells in dlPFC, where low doses of Ro25-6981 dramatically reduced firing, while low doses of CNQX had only subtle effects (Fig. 4B; control vs. Ro, two-tailed paired *t*-test, tdep(7) = −8.4758, $P < 0.001$, $n = 8$; control vs. CNQX, two-tailed paired *t*-test, tdep(7) = −3.1071, $P < 0.05$, $n = 8$). Interestingly, the visual responses of dlPFC Cue cells were reduced by both CNQX and Ro at low doses (Fig. 4C; control vs. Ro, two-tailed paired *t*-test, tdep(3) = −13.3811, $P < 0.001$, $n = 4$; control vs. CNQX, two-tailed paired *t*-test, tdep(4) = −13.3416, $P < 0.001$, $n = 5$), suggesting that Cue cells in dlPFC have characteristics of both dlPFC Delay cells (NMDAR-NR2B sensitivity) and V1 neurons (AMPAR/KR sensitivity).

Role of cAMP-PKA Signaling

The effects of cAMP-PKA signaling on V1 neuronal firing are of particular interest, given the importance of these actions in dlPFC circuits. We iontophoretically applied the cell-permeable, cAMP analog, 8-Br-cAMP sodium salt (8-Br) to activate cAMP-PKA signaling in V1. In the example neuron illustrated in Figure 5A,B, 8-Br produced a dose-related increase in the magnitude of evoked visual responses. High doses of 8-Br (50 nA) significantly enhanced the visual responses (Fig. 5A,B; control vs. 50 nA, one-way ANOVA, $F_{1,2075} = 37.64$, $P < 0.001$). This enhancement was reduced once drug application ceased (Fig. 5A,B; recovery vs. 50 nA, one-way ANOVA, $F_{1,1955} = 21.9319$, $P < 0.001$). At the population level, low doses of 8-Br (10–20 nA) produced a small, but nonsignificant, increase in responsivity (Fig. 5C; control vs. low dose 8-Br, two-tailed paired *t*-test, tdep(13) = 2.0221, $P = 0.069$, $n = 14$), while higher doses (30–50 nA) significantly increased neuronal firing (Fig. 5D; control vs. high dose 8-Br, two-tailed paired *t*-test, tdep(22) = 5.763, $P < 0.001$, $n = 23$). The high doses of 8-Br that increased visually evoked firing also increased spontaneous firing, but to a much lesser extent than sensory-evoked firing (spontaneous, 158.99 ± 14.98%; visually evoked, 173.85 ± 20.47%; spontaneous vs. visually evoked, two-tailed paired *t*-test, tdep(22) = 3.9726, $P < 0.001$, $n = 23$). Firing significantly decreased toward control levels following cessation of drug application (Fig. 5D; recovery vs. high dose 8-Br, two-tailed paired *t*-test, tdep(22) = 3.232, $P < 0.01$, $n = 23$). As illustrated in Figure 5B, 8-Br had similar effects on neuronal firing to luminance increment and decrements (On response, 160.53 ± 15.17%; Off response, 158.01 ± 15.21%; On response vs. Off response, two-tailed paired *t*-test, tdep(22) = 0.6694, $P = 0.5102$, $n = 23$).

The effects of 8-Br on V1 neurons were opposite from those on dlPFC Delay cells, where low 8-Br doses reduced task-related firing (Fig. 5E; control vs. low dose 8-Br in dlPFC, two-tailed paired *t*-test, tdep(17) = 7.1645, $P < 0.001$, $n = 18$; control vs. low dose 8-Br in V1, two-tailed paired *t*-test, tdep(13) = 2.0221, $P = 0.069$, $n = 14$; control vs. high dose 8-Br in V1, two-tailed paired *t*-test, tdep(22) = 5.763, $P < 0.001$, $n = 23$; low dose 8-Br in V1 vs. dlPFC, two-sample *t*-test, tdep(30) = 5.1324, $P < 0.001$, $n = 32$), likely due to increased HCN and KCNQ channel signaling on spines (Arnsten 2015).

Role of HCN Channels

We blocked h-currents in V1 using iontophoretic application of the HCN channel blocker, ZD7288 (ZD), which produced a dose-related reduction in activity. As shown in an example neuron (Fig. 6A,B), ZD at low doses (10 nA) had minimal effects, but at higher doses (30 nA), we observed substantial reductions in visual responses (Fig. 6A; control vs. 30 nA, one-way ANOVA, $F_{1,2594} = 101.9516$, $P < 0.001$). Responses recovered once drug application ceased (Fig. 6A,B; recovery vs. 30 nA, one-way ANOVA, $F_{1,3108} = 51.2565$, $P < 0.001$). Across the population of neurons, low doses of ZD (5–15 nA) had no significant effect on firing (Fig. 6C; control vs. low dose ZD, two-tailed paired *t*-test, tdep(29) = −0.3612, $P = 0.7206$, $n = 30$), while higher doses (20–60 nA) significantly decreased firing (Fig. 6D; control vs. high dose ZD, two-tailed paired t-test, tdep(34) = 5.956, $P < 0.001$, $n = 35$). The high dose of ZD that decreased visually evoked firing also decreased spontaneous firing, but to a much lesser extent (spontaneous, 75.29 ± 4.53%; visually evoked, 70.52 ± 3.48%; spontaneous vs. visually evoked, two-tailed paired *t*-test, tdep(34) = 4.2615, $P < 0.001$, $n = 35$). As with the example neuron, firing returned to baseline levels following cessation of drug application (Fig. 6D; recovery vs. high dose ZD, two-tailed paired *t*-test, tdep(34) = 4.674, $P < 0.001$, $n = 35$). The effects of ZD on luminance increment and decrement stimuli were similar (On response, 72.13 ± 3.72%; Off response, 69.76 ± 3.45%; On response vs. Off response, two-tailed paired *t*-test, tdep(34) = 1.6922, $P = 0.0998$, $n = 35$), as illustrated in Figure 6B. Altogether, these data suggest that HCN channels serve to increase V1 neuronal firing under endogenous conditions, and that their blockade reduces neuronal firing.

The effects of ZD on V1 neurons were different than its effects on dlPFC Delay neurons. While low doses of ZD (5–15 nA) had no effect in V1, the same low doses consistently increased the task-related firing of dlPFC Delay cells (Fig. 6E; low dose ZD in V1 vs. dlPFC, two-sample *t*-test, tdep(55) = −2.5271, $P < 0.05$, $n = 56$). However, the highest doses of ZD (40–60 nA) reduced firing in both V1 and dlPFC neurons (Fig. 6F; high dose ZD in V1 vs. dlPFC, two-sample *t*-test, tdep(22) = 1.1662, $P = 0.256$, $n = 23$).

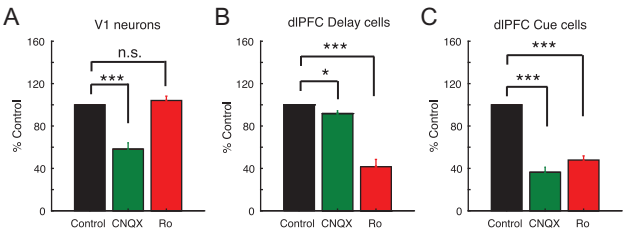

Figure 4. Comparison of low doses of AMPA and NMDA-NR2B antagonists on the firing of V1 versus dlPFC neurons. (*A*) V1 neurons. Low doses (20–25 nA) of CNQX reduced firing to 58% of control values ($P < 0.001$, $n = 10$), while the same dose of Ro ($n = 11$) had no significant effect on V1 neuronal firing. (*B*) dlPFC Delay cells. Low doses (20–25 nA) of CNQX produced only a slight reduction in Delay cell firing ($P < 0.05$), while the same dose of Ro markedly reduced firing ($P < 0.001$). (*C*) dlPFC Cue cells. Low doses (20–25 nA) of CNQX or Ro both reduced the firing of dlPFC Cue cells, which fire only during presentation, similar to V1 neurons. The dlPFC data are from Wang et al. (2013). *$P < 0.05$, ***$P < 0.001$, n.s., nonsignificant.

Immunoelectron Microscopy

Pre-embedding immunoEM was used to examine the subcellular locations of PDE4A and HCN channels in layer III of macaque V1, in order to directly compare results in V1 with previously published data from layer III of dlPFC (please note that this method is not appropriate for visualization of NMDAR and AMPAR).

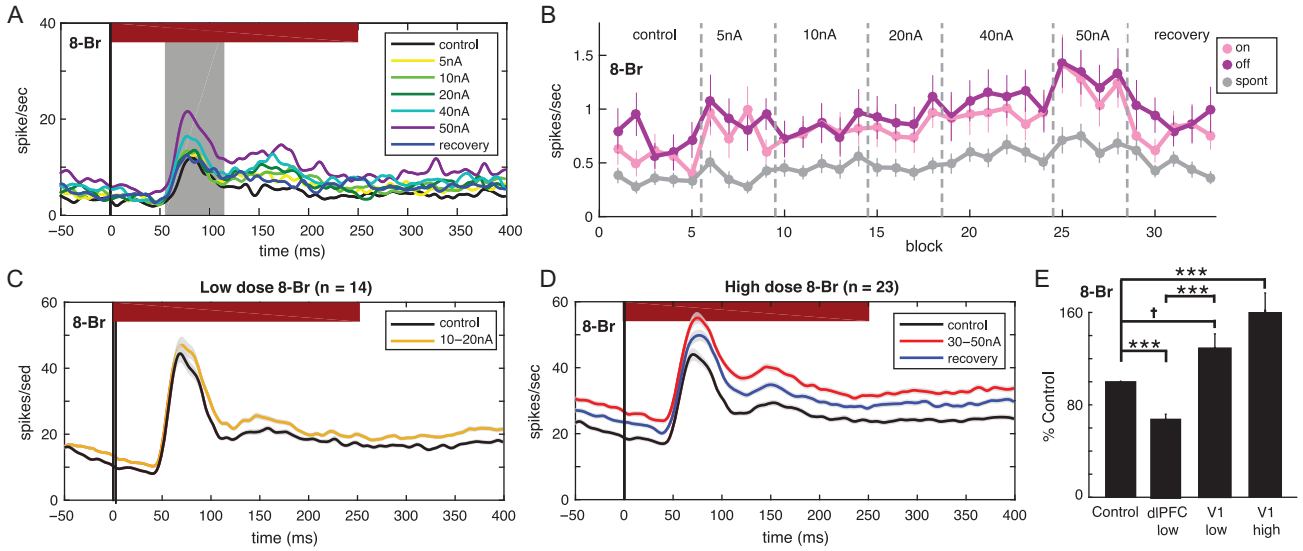

Figure 5. Iontophoresis of the cAMP analog, 8-Bromo-cAMP (8-Br), enhanced visual responses in V1. (*A*) An example neuron showing the effects of increasing doses of 8-Br (5–50 nA) on neuronal firing. The highest dose of 8-Br (50 nA, dark purple) significantly enhanced the visual response (control vs. 50 nA, one-way ANOVA, $F_{1,2075} = 37.64$, $P < 0.001$); this increase was reduced when drug was removed (recovery vs. 50 nA, one-way ANOVA, $F_{1,1955} = 21.9319$, $P < 0.001$). (*B*) The same cell as in (*A*), showing firing dynamics during application of increasing doses of 8-Br. (*C*) Population analysis (average of 14 neurons) of low doses of 8-Br. Low doses of 8-Br (10–20 nA) produced a small, nonsignificant increase in neuronal firing (control vs. low dose 8-Br, two-tailed paired *t*-test, tdep(13) = 2.0221, $P = 0.069$, $n = 14$). Black, control; gold, low dose of 8-Br. (*D*) Population analysis (average of 23 neurons) to high doses of 8-Br. Higher doses (30–50 nA) significantly increased neuronal firing (control vs. high dose 8-Br, two-tailed paired *t*-test, tdep(22) = 5.76, $P < 0.001$, $n = 23$); firing significantly decreased following removal of drug (recovery vs high dose 8-Br, two-tailed paired *t*-test, tdep(22) = 3.232, $P < 0.01$, $n = 23$). Black, control; Red, high dose of 8-Br; Blue, recovery. (*E*) Comparison of 8-Br on the firing of V1 neurons and dlPFC Delay cells. The effects of 8-Br on V1 neurons were opposite from those on dlPFC Delay cells. dlPFC low, low dose 8-Br in dlPFC; V1 low, low dose 8-Br in V1; V1 high, high dose 8-Br in V1. ***$P < 0.001$, †$P = 0.069$.

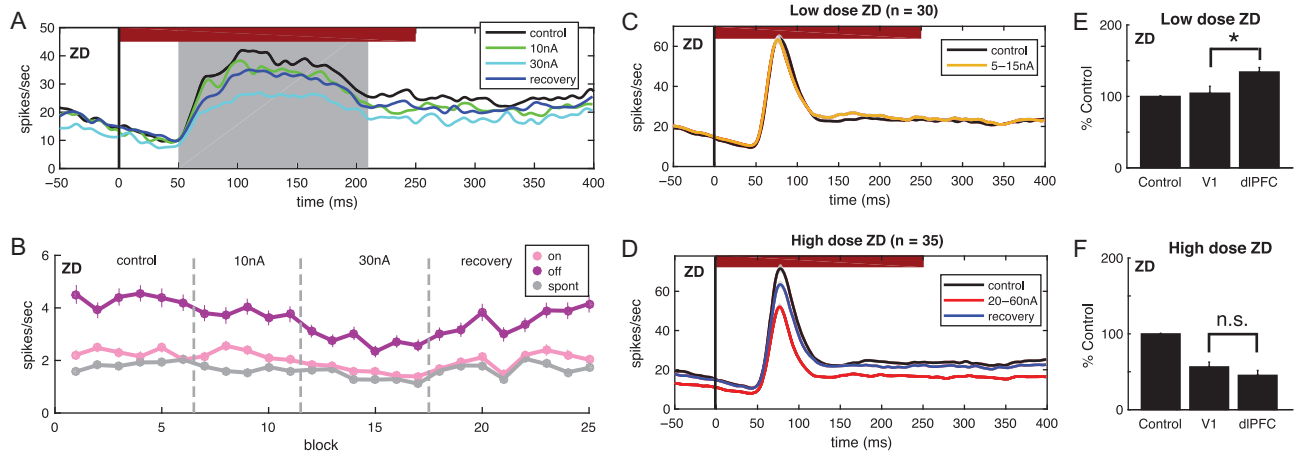

Figure 6. Iontophoresis of the HCN channel blocker, ZD7288 (ZD), decreased visual responses in V1. (*A*) An example neuron showing the effects of increasing doses of ZD (10–30 nA) on neuronal firing. The highest dose of ZD (30 nA, cyan) significantly decreased the visual response (control vs. 30 nA, one-way ANOVA, $F_{1,2594} = 101.9516$, $P < 0.001$); this decrease was recovered when drug was removed (recovery vs. 30 nA, one-way ANOVA, $F_{1,3108} = 51.2565$, $P < 0.001$). (*B*) The same cell as in (*A*), showing firing dynamics during application of increasing doses of ZD. (*C*) Population analysis (average of 30 neurons) of low doses of ZD. Low doses of ZD (5–15 nA) had no effect on neuronal firing (control vs. low dose ZD, two-tailed paired *t*-test, tdep(29) = 0.3612, $P = 0.7206$, $n = 30$). Black, control; Gold, low dose of ZD. (*D*) Population analysis (average of 35 neurons) to high doses of ZD. Higher doses (20–60 nA) significantly decreased neuronal firing (control vs. high dose ZD, two-tailed paired *t*-test, tdep(34) = 5.956, $P < 0.001$, $n = 35$); firing significantly increased following removal of drug (recovery vs. high dose ZD, two-tailed paired *t*-test, tdep(34) = 4.674, $P < 0.001$, $n = 35$). Black, control; red, high dose of ZD; blue, recovery. (*E*) Comparison of low dose of ZD on the firing of V1 neurons and dlPFC Delay cells. (*F*) Comparison of high dose of ZD on the firing of V1 neurons and dlPFC Delay cells. *$P < 0.05$, n.s., nonsignificant.

Ultrastructural Localization of the Phosphodiesterase PDE4A

In macaque V1, PDE4A was predominately localized to axons in layer III (summarized in Fig. 7), with very limited postsynaptic expression (Fig. 7*H*). Within axons, PDE4A was found near the plasma membrane and surrounding putative glutamate vesicles (based on morphology) in both intervaricose axonal segments (Fig. 7A–C, G), and in presynaptic terminals (Fig. 7D–F). Thus, PDE4A is well-positioned to regulate cAMP-mediated facilitation of glutamate release, including volume release at nonsynaptic sites from intervaricose segments. These immunoEM findings are consistent with the physiological findings described above demonstrating that cAMP signaling increases V1 activity, consistent with increased glutamate release.

A small fraction of PDE4A also was detected postsynaptically: in dendrites, mushroom-shaped spines (Fig. 7G,H) and glia (not shown). PDE4A was present over the spine apparatus in mushroom spines, positioned to regulate cAMP modulation of internal calcium release. In contrast to dlPFC, PDE4A in V1 was rarely observed in thin spines, its primary location in dlPFC. This pattern of PDE4A expression in macaque V1 layer III is markedly different from that in dlPFC, where PDE4A is predominately found postsynaptically in thin-type spines.

Ultrastructural Localization of HCN1 Channels

HCN1 channels in primate V1 are concentrated on distal dendrites (Fig. 8), the classical pattern for cortical HCN expression. Figure 8A shows a typical V1 layer III pyramidal cell where the density of expression on the apical dendrite increases with distance from the soma (Fig. 8B), reaching maximal levels in layer I dendritic branches (Fig. 8C). ImmunoEM confirmed this pattern, with the majority of label localized on dendritic membranes and trafficking on dendritic microtubules (Fig. 8D,E). Like PDE4A, HCN channels were occasionally observed on the membranes of mushroom spines, but not thin spines (Fig. 8F), and were commonly seen in glutamatergic-like axon terminals at both perisynaptic and extrasynaptic locations (Fig. 8G,H). The marked reduction in V1 neuronal firing following HCN channel blockade is consistent with this profile, where HCN1-mediated hyperpolarization of dendrites would likely attenuate neuronal responses.

Discussion

This study of V1 neurons in rhesus macaques performing a visual fixation task found that stimulus-evoked neuronal firing relies primarily on glutamate stimulation of AMPAR/KR, with a more subtle contribution of NMDAR, and that cAMP-PKA and HCN channel signaling both have facilitatory effects on neuronal firing. This profile is opposite to that found in studies of dlPFC Delay cells, where firing depends more on NMDAR than AMPAR/KR stimulation, and cAMP and HCN channel signaling both reduce firing. The intracellular localization of PDE4A and HCN channels also differed between cortical regions. In V1, PDE4A was concentrated presynaptically in axon terminals, while in dlPFC PDE4A was prominent postsynaptically in thin-type dendritic spines, near HCN channels in the spine membrane. In contrast, HCN channels in V1 were found in their classical location on distal dendrites. These results indicate that primate V1 neurons are regulated in a classical manner, which differs remarkably from

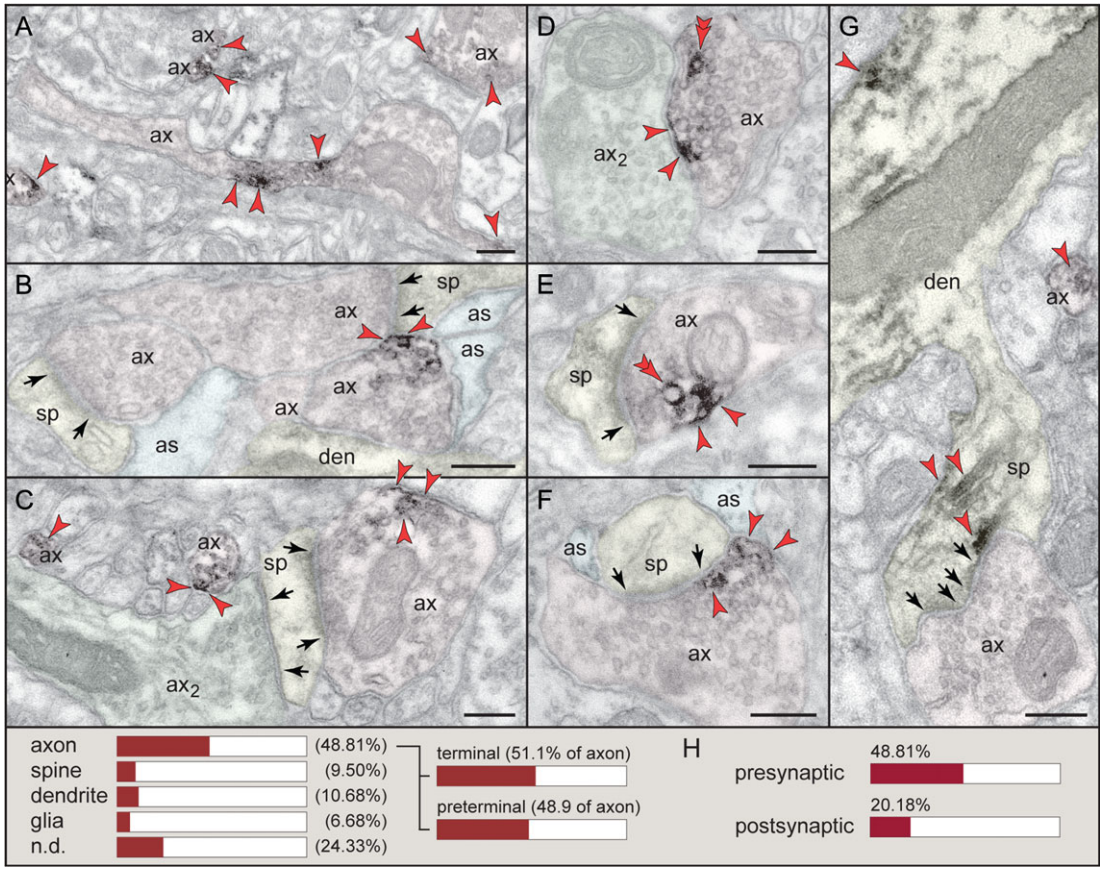

Figure 7. PDE4A in monkey V1 is predominantly presynaptic. (*A–F*) PDE4A (red arrowheads) is expressed in glutamatergic-like terminal and preterminal (intervaricose) segments of axons (pink pseudocolored); compare with the nonglutamatergic-like ax2 (green-pseudocolored) in *C* and *D*. Note that PDE4A appears at nonsynaptic axonal membranes, and rarely perisynaptically (*F*). In addition to the plasma membrane, PDE4A is found on vesicular endomembranes (double red arrowheads in *D* and *E*). (*G*) Postsynaptic PDE4A is found in the spines and the shaft of dendrites (yellow-pseudocolored). In spines, PDE4A is perisynaptic and extrasynaptic, and associates with the spine apparatus. (*H*) Prevalence of PDE4A in various cellular profiles in layer III of V1 neuropil; expressed as percentage of a PDE4A profile (e.g., axon) per total PDE4A profiles (see quantitative assessment in Materials and Methods). Nondetermined (n.d.) are profiles that could not be unequivocally categorized. PDE4A is foremost expressed in terminal and preterminal axons. There is a smaller postsynaptic component in dendritic spines and shafts as well as a limited glial component. as, astrocyte; ax, axon; den, dendrite; sp, spine. Synapses are between arrows. Scale bars, 200 nm.

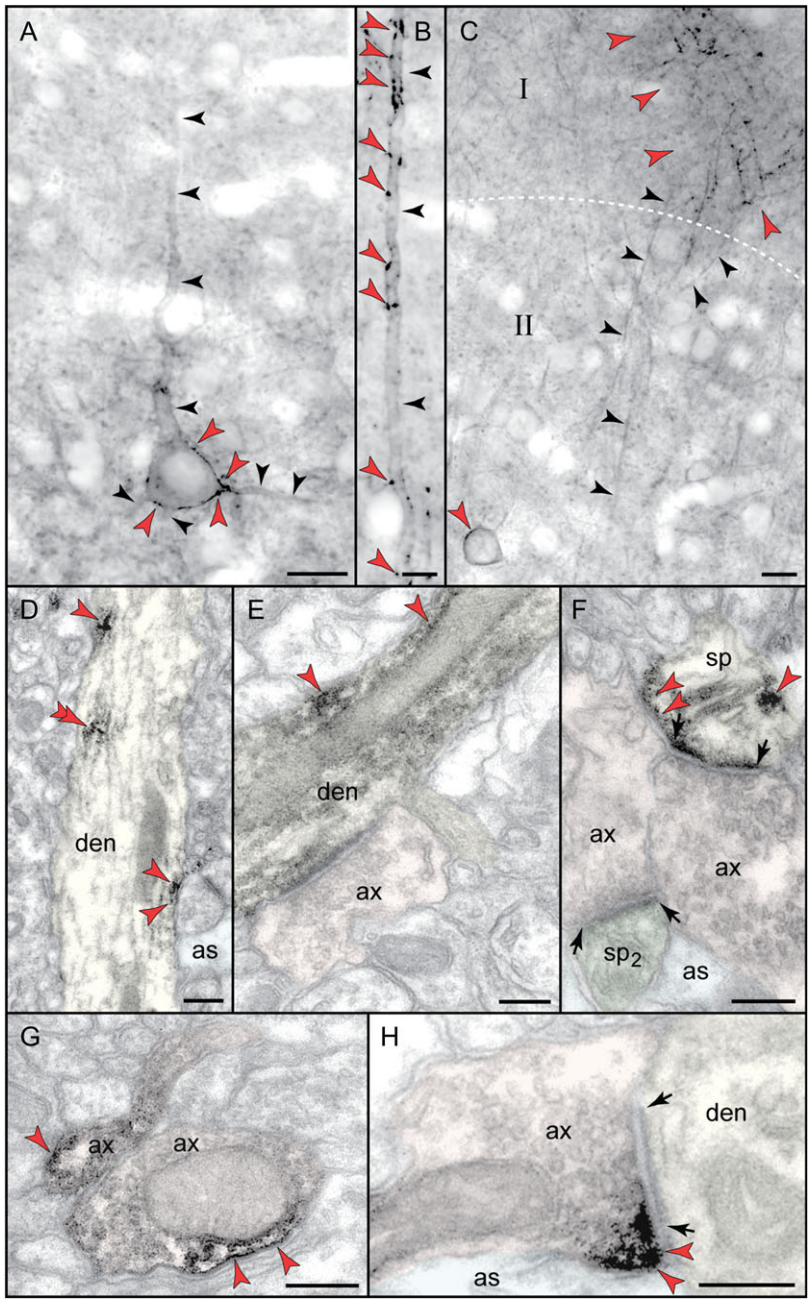

Figure 8. HCN1 Channels in Monkey V1. (*A–C*) HCN1 channels (red arrowheads) are found in pyramidal neurons in layer III V1; black arrowheads point to the apical and basal dendrites (*A*). Channel expression along the pyramidal apical dendrite increases with distance from the soma (*B*), reaching maximal levels in the dendritic tufts that ramify into layer I (*C*). (*D*, *E*) Ultrastructurally, HCN1 channels are typically captured at the plasma membrane of dendritic shafts (yellow-pseudocolored); intracellular labeling likely represents channels en passant (double red arrowheads in *D*). (*F*) Channels were also found in spines, predominantly of the mushroom-type; compare with the nonreactive, thin-type sp2 (green-pseudocolored) in the same panel. (*G*, *H*) A presynaptic HCN1 channel component was detected in glutamatergic-like axons (pink-pseudocolored). Labeling appeared along nonsynaptic axonal membranes (*G*), and perisynaptically to asymmetric, excitatory-like synapses (*H*). as, astrocyte; ax, axon; den, dendrite; sp, spine. Synapses are between arrows. Scale bars, 10 μm (*A–C*); 200 nm (*D–H*).

mechanisms governing the more recently evolved circuits in primate dlPFC.

A weakness of in vivo studies of this kind is the inability to identify the exact neuronal subtype or its laminar location within V1. The slow, regular pattern of firing of most neurons examined would be consistent with pyramidal cells, or nonfast-spiking interneurons, and thus, it is likely that a large proportion of neurons studied here were pyramidal cells. However, the data are insufficient to distinguish neuronal subtypes or lamina of origin.

Glutamate Receptor Actions in V1

The current study found potent reductions in V1 firing following AMPAR/KR blockade, while NMDAR blockade required substantially higher doses. This differential sensitivity between AMPAR/KR versus NMDAR may arise from a number of factors, for example, there may be fewer NMDAR than AMPAR/KR within the PSD, and/or, if the primate V1 is similar to perinatal rodent V1, blockade of presynaptic NMDAR may increase

glutamate release and oppose the postsynaptic actions (Li et al. 2009). Drug effects were more prominent for sensory-evoked than for spontaneous firing, although higher doses did affect spontaneous activity as well as visually evoked responses. These data suggest that basal circuit dynamics are qualitatively similar to those during sensory stimulation, when activity is amplified by feedforward, sensory stimulation.

The current effects of glutamate receptor antagonist application reported here are consistent with those from previous studies of primate V1, which utilized more attention-demanding tasks. Earlier studies have found that AMPAR/KR stimulation is a major component of "bottom-up" processing, while NMDAR stimulation is more important for "top-down" actions such as figure/ground processing (Self et al. 2012), and attentional modulation (i.e., attention-induced reductions in response variability and noise correlation) (Herrero et al. 2013). Directly pertinent to the current study, Self et al. (2012) found that "bottom-up" (feedforward), visually driven activity was strongly reduced by CNQX but not by NMDAR antagonists. Self et al. differed from the current experiments in several ways: the visual "figure" stimulus was embedded in a textured background pattern, different NMDAR modulators were used, and the drugs were injected rather than iontophoresed. Nonetheless, CNQX produced a similar reduction in firing (to about 60% of control) in both studies, which recovered once drug was no longer applied. Self et al. also found more subtle effects of NMDAR blockade than AMPAR blockade on sensory-evoked activity. Blockade of all NMDAR with APV produced only a slight reduction in the visually evoked response (~7–8%), and NMDAR-NR2B blockade with ifenprodil actually produced a small increase in sensory-driven firing (~8%) (Self et al. 2012). However, since ifenprodil is nonselective, for example, blocking GIRK potassium channels (Kobayashi et al. 2006), its excitatory effects on V1 neurons may not be mediated by NMDAR. This hypothesis is suggested by results from the current study, where the more selective NMDAR-NR2B antagonist, Ro25-6981 (Fischer et al. 1997) did not increase V1 neuronal firing, although the balance of presynaptic versus postsynaptic actions may account for small discrepancies between studies. However, overall the results of these 2 studies are remarkably similar, emphasizing the key role of AMPAR/KR in the "bottom-up" processing of visual stimuli in the primary visual cortex. As AMPAR have faster kinetics than NMDAR (Kleppe and Robinson 1999 and Robinson 1999 and Robinson 1999), they may be more appropriate for the rapid, faithful following of sensory stimulation.

Excitatory Effects of cAMP-HCN Channel Signaling in Primate V1

To our knowledge, this is the first study of cAMP- and HCN channel signaling in primate V1. We should caution that PDE4A does not serve as a comprehensive index of cAMP signaling localization, but is of great interest given its localization in layer III dlPFC, where both PDE4A and HCN channels are very prevalent in mature, thin-type spines (Paspalas et al. 2013), forming a "signature of flexibility" for postsynaptic gating that reduces cell firing (Arnsten et al. 2012). The data indicate a very different picture in primate V1, where cAMP-PKA signaling and HCN channels have classical excitatory actions, similar to those found in rodent sensory cortex.

PDE4A expression was predominately observed in glutamate-like axons in primate V1 layer III, surrounding synaptic vesicles in both axon terminals (at axo-spinous and axo-axonal interactions), and in intervaricose segments, which are sites of glutamate volume release. cAMP-PKA signaling is known to enhance transmitter release (Greengard et al. 1991; Valtorta and Meldolesi 1994; Hosaka et al. 1999), for example, via phosphorylation of SNAP-25 on vesicles (Nagy et al. 2004). Thus, the current data indicate that cAMP signaling proteins are positioned to enhance glutamate release in primate V1. The physiological data support this hypothesis, as the cAMP analog 8-Br-cAMP markedly increased V1 neuronal firing. Firing returned to baseline after drug was removed, consistent with a transient increase in glutamate release rather than a plastic change in excitability associated with LTP.

HCN channels in primate V1 layer III were predominately expressed on the distal portion of apical dendrites, their classic location on pyramidal cells, for example, in rodent somatosensory cortex (Lörincz et al. 2002), where the HCN current (Ih) depolarizes the dendrite in response to membrane hyperpolarization (Fan et al. 2005; He et al. 2014). Presynaptic HCN channels may also depolarize the axon terminal and enhance transmitter release (Southan et al. 2000). The current study found that blockade of HCN channels in primate V1 with ZD7288 reduced neuronal firing, consistent with these classic actions. Interestingly, research in mouse V1 indicates that suppression of Ih contributes to reduced neuronal firing with some types of anesthesia (Chen et al. 2005, 2009).

In contrast to dlPFC, neither HCN1 nor PDE4A were commonly expressed in spines, and spine expression was limited to mushroom-type, not thin-type spines. Expression in mushroom-type spines may reflect a classical cAMP role in plasticity, a focus of previous research in rodent V1, for example, in regard to the development of ocular dominance columns (Hensch et al. 1998). However, mushroom spines comprise a surprisingly small proportion of spines in adult primate V1 layer III: mushroom-type ~9%, stubby-type ~23%, thin-type ~68% (Young et al. 2014). Thus, the minor expression of PDE4A and HCN channels in mushroom spines is consistent with the small numbers of these spines in primate V1 layer III.

Comparing V1 to dlPFC

The current study purposefully utilized the same methods, drugs, doses, and molecular targets previously used to study dlPFC neurons, thus allowing direct comparison between these 2 cortical regions. V1 and dlPFC have opposing functions: V1 processes visual stimuli as they occur, while dlPFC, particularly dlPFC Delay cells, represents visual stimuli in their absence (Arnsten et al. 2012). Thus, it is of interest to compare V1 neurons to Delay cells, which are able to sustain firing across the delay period in the absence of a visual cue, and to dlPFC Cue cells, which like V1 neurons, only fire during stimulus presentation.

The persistent firing of dlPFC Delay cells depends on NMDAR stimulation, but is only subtly altered by AMPAR/KR blockade (Wang et al. 2013). In particular, Delay cells rely on NMDAR with NR2B subunits, which are localized exclusively within the PSD in dlPFC (Wang et al. 2013). This profile contrasts with V1 neurons, where AMPAR/KR blockade markedly reduced firing, while NMDAR-NR2B blockade had much less potent effects. NMDAR actions classically require AMPAR depolarization of the membrane to relieve the magnesium block, and it is likely that AMPAR perform this key function in V1 neurons. In contrast, these permissive actions in dlPFC Delay cells are performed by cholinergic stimulation of nicotinic α7 receptors, such that network connectivity is greatly determined by arousal state (Yang et al. 2013). To date, there is no evidence that nicotinic alpha-7 receptors influence V1 neuronal firing, although acetylcholine plays an important role via muscarinic and β-nicotinic receptor mechanisms

(Disney et al. 2007; Herrero et al. 2008; Soma et al. 2012; Shimegi et al. 2016). Thus, basic neurotransmission differs markedly between V1 and dlPFC Delay cells.

In contrast to dlPFC Delay cells, dlPFC Cue cells have properties of both V1 neurons and dlPFC Delay cells, that is, dlPFC Cue cells are dependent on AMPAR/KR actions (Wang et al. 2013), but are also very sensitive to NMDAR-NR2B blockade. Overall, these data suggest that AMPAR/KR may be essential for neurotransmission in circuits where there is a need for (1) rapid, temporally accurate neuronal response; and/or (2) circuit activity to reflect the occurrence of an event more than arousal state, for example, the degree of AMPAR stimulation, not acetylcholine release, determines NMDAR opening. In contrast, layer III dlPFC circuits require the slower kinetics of NMDAR-NR2B to sustain persistent firing (Wang 1999), and acetylcholine release during wakefulness permits conscious, cognitive processing (Yang et al. 2013).

As with glutamate transmission, cAMP-HCN channel signaling also has opposing influences in V1 versus dlPFC Delay cells, where cAMP-PKA signaling and HCN channel actions are excitatory in V1, but decrease Delay cell firing in dlPFC. These physiological data are consistent with the differential localization of these proteins in V1 versus dlPFC, where PDE4A is predominately axonal and HCN channels concentrate on distal dendrites in layer III V1 neurons. In contrast, PDE4A and HCN channels are colocalized in mature, thin-type spines in layer III of dlPFC (Paspalas et al. 2013), which predominate in layer III dlPFC circuits (~67%) (Young et al. 2014). (It should be noted that the thin-type spines in both V1 and dlPFC are not the immature "learning" spines seen in vitro, but rather have mature characteristics such as a well-defined PSD and often a spine apparatus (Bourne and Harris 2007).) In dlPFC, PDE4A is anchored to the calcium-storing spine apparatus by DISC1 (Paspalas et al. 2013; Carlyle et al. 2014), where feedforward calcium-cAMP-HCN channel signaling weakens connectivity and reduces Delay cell firing (Wang et al. 2007). Thus, low doses of the HCN channel blocker, ZD7288, enhance the firing of dlPFC cells (Wang et al. 2007), but have no effect on V1 neurons. Higher doses of ZD7288, presumably needed to effectively block the extensive expression of HCN channels on dendrites, reduced firing of both V1 and dlPFC cells. However, the paucity of HCN channel expression on spines in V1 may be a key difference between these 2 regions, helping to explain why stress and disease readily weaken dlPFC connectivity, while V1 circuits are more resilient.

Relevance to Resilience of V1 Neurons

The differences between V1 and dlPFC found in the current study may help explain why these areas show such varied responses to stress and/or inflammation. Both stress and inflammation can drive cAMP signaling, where stress induces high levels of monoamine release that activate Gs-coupled receptors (e.g., via dopamine D1 receptors), while inflammation inhibits PDE4 activity through MK2 signaling (MacKenzie et al. 2011). These molecular events would increase neuronal firing in V1, but weaken connectivity and reduce Delay cell firing in dlPFC via cAMP-HCN channel actions in spines (Arnsten 2015). When these mechanisms are engaged over long periods of time, as in chronic stress or advancing age, they contribute to loss of synapses and increased phosphorylation of tau (Carlyle et al. 2014; Hains et al. 2015). In contrast, there is very little spine loss in V1 with advancing age (Luebke et al. 2013; Young et al. 2014), and V1 is the last cortical region to be afflicted in Alzheimer's disease (Lewis et al. 1987; Braak and Braak 1995). The resilience of the primary visual cortex may be due in part to its molecular regulation, where cAMP signaling and HCN channel opening strengthen, rather than weaken, neuronal firing. V1's lesser dependence on NMDAR-NR2B may also be protective, given the large calcium flux through these channels. Taken together, these mechanistic differences may begin to explain why V1 neurons are so resistant to the deleterious effects of stress and age.

Authors' Contributions

S.-T.Y., M.W., C.D.P., J.A.M., and A.F.T.A. conceived and designed the project, S.-T.Y., M.W., C.D.P., J.L.C., and M.A. performed experiments. S.-T.Y., J.A.M., M.W., C.D.P., J.L.C., and M.A. analyzed data, S.-T.Y., M.W., C.D.P., J.A.M., and A.F.T.A. wrote the article.

Funding

National Institutes of Health Director's Pioneer Award to A.F.T.A. (DP1-AG047744-01) and National Eye Institute Award to J.A.M (EY025103).

Notes

We thank L. Ciavarella, S. Johnson, T. Sadlon, M. Wilson, and M. Horn for invaluable technical support. *Conflict of Interest*: None declared.

References

Arnsten AF. 2015. Stress weakens prefrontal networks: molecular insults to higher cognition. Nat Neurosci. 18:1376–1385.

Arnsten AFT, Wang M, Paspalas CD. 2012. Neuromodulation of thought: flexibilities and vulnerabilities in prefrontal cortical network synapses. Neuron. 76:223–239.

Bair W, Cavanaugh JR, Smith MA, Movshon JA. 2002. The timing of response onset and offset in macaque visual neurons. J Neurosci. 22:3189–3205.

Berardi N, Pizzorusso T, Ratto GM, Maffei L. 2003. Molecular basis of plasticity in the visual cortex. Trends Neurosci. 26: 369–378.

Bourne J, Harris KM. 2007. Do thin spines learn to be mushroom spines that remember? Curr Opin Neurobiol. 17:381–386.

Braak H, Braak E. 1995. Staging of Alzheimer's disease-related neurofibrillary changes. Neurobiol Aging. 16:271–278.

Carlyle BC, Nairn AC, Wang M, Yang Y, Jin LE, Simen AA, Ramos BP, Bordner KA, Craft GE, Davies P, et al. 2014. cAMP-PKA phosphorylation of tau confers risk for degeneration in aging association cortex. Proc Natl Acad Sci USA. 111:5036–5041.

Chen X, Shu S, Bayliss DA. 2005. Suppression of ih contributes to propofol-induced inhibition of mouse cortical pyramidal neurons. J Neurophysiol. 94:3872–3883.

Chen X, Shu S, Kennedy DP, Willcox SC, Bayliss DA. 2009. Subunit-specific effects of isoflurane on neuronal Ih in HCN1 knockout mice. J Neurophysiol. 101:129–140.

Disney AA, Aoki C, Hawken MJ. 2007. Gain modulation by nicotine in macaque v1. Neuron. 56:701–713.

Fan Y, Fricker D, Brager DH, Chen X, Lu HC, Chitwood RA, Johnston D. 2005. Activity-dependent decrease of excitability in rat hippocampal neurons through increases in I(h). Nat Neurosci. 8:1542–1551.

Fischer G, Mutel V, Trube G, Malherbe P, Kew JN, Mohacsi E, Heitz MP, Kemp JA. 1997. Ro 25–6981, a highly potent and

selective blocker of N-methyl-D-aspartate receptors containing the NR2B subunit. Characterization in vitro. J Pharmacol Exp Ther. 283:1285–1292.

Funahashi S, Bruce CJ, Goldman-Rakic PS. 1989. Mnemonic coding of visual space in the monkey's dorsolateral prefrontal cortex. J Neurophysiol. 61:331–349.

Gamo NJ, Lur G, Higley MJ, Wang M, Paspalas CD, Vijayraghavan S, Yang Y, Ramos BP, Peng K, Kata A, et al. 2015. Stress impairs prefrontal cortical function via D1 dopamine receptor interactions with HCN channels. Biol Psychiatry. 78:860–870.

Glantz LA, Lewis DA. 2000. Decreased dendritic spine density on prefrontal cortical pyramidal neurons in schizophrenia. Arch Gen Psychiatry. 57:65–73.

Goldman-Rakic PS. 1995. Cellular basis of working memory. Neuron. 14:477–485.

Greengard P, Jen J, Nairn AC, Stevens CF. 1991. Enhancement of the glutamate response by cAMP-dependent protein kinase in hippocampal neurons. Science. 253:1135–1138.

Hains AB, Vu MA, Maciejewski PK, van Dyck CH, Gottron M, Arnsten AF. 2009. Inhibition of protein kinase C signaling protects prefrontal cortex dendritic spines and cognition from the effects of chronic stress. Proc Natl Acad Sci USA. 106:17957–17962.

Hains AB, Yabe Y, Arnsten AFT. 2015. Chronic stimulation of alpha-2A-adrenoceptors with guanfacine protects rodent prefrontal cortex dendritic spines and cognition from the effects of chronic stress. Neurobiol Stress. 2:1–9.

He C, Chen F, Li B, Hu Z. 2014. Neurophysiology of HCN channels: from cellular functions to multiple regulations. Prog Neurobiol. 112:1–23.

Hensch TK, Gordon JA, Brandon EP, McKnight GS, Idzerda RL, Stryker MP. 1998. Comparison of plasticity in vivo and in vitro in the developing visual cortex of normal and protein kinase A RIbeta-deficient mice. J Neurosci. 18: 2108–2117.

Herrero JL, Gieselmann MA, Sanayei M, Thiele A. 2013. Attention-induced variance and noise correlation reduction in macaque V1 is mediated by NMDA receptors. Neuron. 78: 729–739.

Herrero JL, Roberts MJ, Delicato LS, Gieselmann MA, Dayan P, Thiele A. 2008. Acetylcholine contributes through muscarinic receptors to attentional modulation in V1. Nature. 454: 1110–1114.

Hosaka M, Hammer RE, Südhof TC. 1999. A phospho-switch controls the dynamic association of synapsins with synaptic vesicles. Neuron. 24:377–387.

Kleppe IC, Robinson HP. 1999. Determining the activation time course of synaptic AMPA receptors from openings of colocalized NMDA receptors. Biophys J. 77:1418–1427.

Kobayashi T, Washiyama K, Ikeda K. 2006. Inhibition of G protein-activated inwardly rectifying K+ channels by ifenprodil. Neuropsychopharmacology. 31:516–524.

Langdon RB, Sur M. 1992. The effects of selective glutamate receptor antagonists on synchronized firing bursts in layer III of rat visual cortex. Brain Res. 599:283–296.

Lewis DA, Campbell MJ, Terry RD, Morrison JH. 1987. Laminar and regional distributions of neurofibrillary tangles and neuritic plaques in Alzheimer's disease: a quantitative study of visual and auditory cortices. J Neurosci. 7:1799–1808.

Li YH, Wang J. 2013. Membrane insertion of new AMPA receptors and LTP induced by glycine is prevented by blocking NR2A-containing NMDA receptors in the rat visual cortex in vitro. Curr Neurovasc Res. 10:70–75.

Li YH, Wang J, Zhang G. 2009. Presynaptic NR2B-containing NMDA autoreceptors mediate glutamatergic synaptic transmission in the rat visual cortex. Curr Neurovasc Res. 6:104–109.

Liu XB, Murray KD, Jones EG. 2004. Switching of NMDA receptor 2A and 2B subunits at thalamic and cortical synapses during early postnatal development. J Neurosci. 24:8885–8895.

Luebke JI, Medalla M, Amatrudo JM, Weaver CM, Crimins JL, Hunt B, Hof PR, Peters A. 2013. Age-related changes to layer 3 pyramidal cells in the rhesus monkey visual cortex. Cereb Cortex. 25:1454–1468. Dec 8:[Epub ahead of print].

Lörincz A, Notomi T, Tamas G, Shigemoto R, Nusser Z. 2002. Polarized and compartment-dependent distribution of HCN1 in pyramidal cell dendrites. Nat Neurosci. 5:1185–1193.

MacKenzie KF, Wallace DA, Hill EV, Anthony DF, Henderson DJ, Houslay DM, Arthur JS, Baillie GS, Houslay MD. 2011. Phosphorylation of cAMP-specific PDE4A5 (phosphodiesterase-4A5) by MK2 (MAPKAPK2) attenuates its activation through protein kinase A phosphorylation. Biochem J. 435:755–769.

Mazer JA, Vinje WE, McDermott J, Schiller PH, Gallant JL. 2002. Spatial frequency and orientation tuning dynamics in area V1. Proc Natl Acad Sci USA. 99:1645–1650.

Myme CI, Sugino K, Turrigiano GG, Nelson SB. 2003. The NMDA-to-AMPA ratio at synapses onto layer 2/3 pyramidal neurons is conserved across prefrontal and visual cortices. J Neurophysiol. 90:771–779.

Nagy G, Reim K, Matti U, Brose N, Binz T, Rettig J, Neher E, Sørensen JB. 2004. Regulation of releasable vesicle pool sizes by protein kinase A-dependent phosphorylation of SNAP-25. Neuron. 41:417–429.

Nase G, Weishaupt J, Stern P, Singer W, Monyer H. 1999. Genetic and epigenetic regulation of NMDA receptor expression in the rat visual cortex. Eur J Neurosci. 11: 4320–4326.

Paspalas CD, Min Wang M, Arnsten AFT. 2013. Constellation of HCN Channels and cAMP regulating proteins in dendritic spines of the primate prefrontal cortex—potential substrate for working memory deficits in schizophrenia. Cereb Cortex. 23:1643–1654.

Self MW, Kooijmans RN, Supèr H, Lamme VA, Roelfsema PR. 2012. Different glutamate receptors convey feedforward and recurrent processing in macaque V1. Proc Natl Acad Sci USA. 109:11031–11036.

Shimegi S, Kimura A, Sato A, Aoyama C, Mizuyama R, Tsunoda K, Ueda F, Araki S, Goya R, Sato H. 2016. Cholinergic and serotonergic modulation of visual information processing in monkey V1. J Physiol Paris. 110:44–51.

Soma S, Shimegi S, Osaki H, Sato H. 2012. Cholinergic modulation of response gain in the primary visual cortex of the macaque. J Neurophysiol. 107:283–291.

Southan AP, Morris NP, Stephens GJ, Robertson B. 2000. Hyperpolarization-activated currents in presynaptic terminals of mouse cerebellar basket cells. J Physiol. 526:91–97.

Touryan J, Mazer JA. 2015. Linear and non-linear properties of feature selectivity in V4 neurons. Front Syst Neurosci. 9:82.

Valtorta F, Meldolesi J. 1994. The presynaptic compartment: signals and targets. Semin Cell Biol. 5:211–219.

van Kerkoerle T, Self MW, Roelfsema PR. 2017. Layer-specificity in the effects of attention and working memory on activity in primary visual cortex. Nat Commun. 8:13804.

Vijayraghavan S, Wang M, Birnbaum SG, Bruce CJ, Williams GV, Arnsten AFT. 2007. Inverted-U dopamine D1 receptor actions on prefrontal neurons engaged in working memory. Nat Neurosci. 10:376–384.

Wang XJ. 1999. Synaptic basis of cortical persistent activity: the importance of NMDA receptors to working memory. J Neurosci. 19:9587–9603.

Wang M, Gamo NJ, Yang Y, Jin LE, Wang XJ, Laubach M, Mazer JA, Lee D, Arnsten AFT. 2011. Neuronal basis of age-related working memory decline. Nature. 476:210–213.

Wang L, Li XJ, Hsiao SS, Lenz FA, Bodner M, Zhou YD, Fuster JM. 2015. Differential roles of delay-period neural activity in the monkey dorsolateral prefrontal cortex in visual-haptic crossmodal working memory. Proc Natl Acad Sci USA. 112: E214–E219.

Wang M, Ramos B, Paspalas C, Shu Y, Simen A, Duque A, Vijayraghavan S, Brennan A, Dudley AG, Nou E, et al. 2007. Alpha2A-adrenoceptor stimulation strengthens working memory networks by inhibiting cAMP-HCN channel signaling in prefrontal cortex. Cell. 129:397–410.

Wang H, Stradtman GGr, Wang XJ, Gao WJ. 2008. A specialized NMDA receptor function in layer 5 recurrent microcircuitry of the adult rat prefrontal cortex. Proc Natl Acad Sci USA. 105:16791–16796.

Wang M, Yang Y, Wang CJ, Gamo NJ, Jin LE, Mazer JA, Morrison JH, Wang X-J, Arnsten AF. 2013. NMDA receptors subserve working memory persistent neuronal firing in dorsolateral prefrontal cortex. Neuron. 77:736–749.

Yang Y, Paspalas CD, Jin LE, Picciotto MR, Arnsten AFT, Wang M. 2013. Nicotinic α7 receptors enhance NMDA cognitive circuits in dorsolateral prefrontal cortex. Proc Nat Acad Sci USA. 110:12078–12083.

Young ME, Ohm DT, Dumitriu D, Rapp PR, Morrison JH. 2014. Differential effects of aging on dendritic spines in visual cortex and prefrontal cortex of the rhesus monkey. Neuroscience. 274:33–43.